Accepted for publication in the Astrophysical Journal

Strong Infrared Emission from the Extrasolar Planet HD 189733b

Drake Deming

Planetary Systems Laboratory, NASA's Goddard Space Flight Center, Mail Code 693, Greenbelt, MD 20771

ddeming@pop600.gsfc.nasa.gov

Joseph Harrington

Center for Radiophysics and Space Research, Cornell University, 326 Space Sciences Bldg., Ithaca, NY 14853-6801

jh@oobleck.astro.cornell.edu

Sara Seager

Department of Terrestrial Magnetism, Carnegie Institution of Washington, 5241 Broad Branch Rd NW, Washington, DC 20015

seager@dtm.ciw.edu

L. Jeremy Richardson[1]

Exoplanets and Stellar Astrophysics Laboratory, NASA's Goddard Space Flight Center, Mail Code 667, Greenbelt, MD 20771

richardsonlj@milkyway.gsfc.nasa.gov

ABSTRACT

We report detection of strong infrared thermal emission from the nearby (d = 19 pc) transiting extrasolar planet HD 189733b, by measuring the flux decrement during its prominent secondary eclipse. A 6-hour photometric sequence using Spitzer's infrared spectrograph in peak-up imaging mode at 16 μm shows the secondary eclipse depth to be $0.551 \pm 0.030\%$, with accuracy limited by

[1]NRC Postdoctoral Research Fellow

instrumental baseline uncertainties, but with 32σ precision ($\sigma = 0.017\%$) on the detection. The 16 μm brightness temperature of this planet (1117 ± 42K) is very similar to the Spitzer detections of TrES-1 and HD 209458b, but the observed planetary flux (660 μJy) is an order of magnitude greater. This large signal will allow a detailed characterization of this planet in the infrared. Our photometry has sufficient signal-to-noise (~ 400 per point) to motivate a search for structure in the ingress/egress portions of the eclipse curve, caused by putative thermal structure on the disk of the planet. We show that by binning our 6-second sampling down to $\sim$ 6-minute resolution, we detect the modulation in the intensity derivative during ingress/egress due to the overall shape of the planet, but our sensitivity is not yet sufficient to distinguish between realistic models of the temperature distribution across the planet's disk. We point out the potential for extending Spitzer secondary eclipse detections down to the regime of transiting hot Neptunes, if such systems are discovered among nearby lower main sequence stars.

Subject headings: stars: individual (HD 189733), stars: planetary systems, infrared: general

1. Introduction

The detection of infrared (IR) thermal emission from two extrasolar planets (Charbonneau et al. 2005; Deming et al. 2005) using the *Spitzer Space Telescope* (Werner et al. 2004) opened a new era in which planets orbiting other stars can be studied directly. The Spitzer detections were made by observing the flux decrement during secondary eclipse in transiting systems. The recently discovered planet transiting the star HD 189733 (Bouchy et al. 2005) is particularly suitable for Spitzer detection and characterization, because it transits a relatively small star – allowing maximum planet-star contrast – and because the distance to the system is only 19 pc (Perryman et al. 1997). HD 189733b has an orbital period of only 2.219 days (Bouchy et al. 2005), putting it in the class of 'very hot Jupiters'. Gaudi et al. (2005) suggested that the very hot Jupiters are a separate dynamical class of exoplanets. Since the other members of this class orbit much fainter stars, the discovery of HD 189733 may allow a previously impossible direct comparison between different classes of extrasolar planets.

In this paper we report detection of a prominent secondary eclipse of HD 189733b using Spitzer observations at 16 μm. We confirm that the strong IR thermal emission from this planet will indeed permit detailed characterization studies. To begin such studies, we examine our data for structure in the ingress/egress portions of the eclipse curve, as can be caused

by temperature structure on the disk of the planet. We thus attempt the first exploratory observations of spatially-resolved structure on the disk of a planet orbiting another star.

2. Observations

Whereas the first Spitzer detections (Charbonneau et al. 2005; Deming et al. 2005) were made using the IRAC and MIPS instruments, we here use the Infrared Spectrograph (IRS, Houck et al. 2004) in the peak-up imaging (PUI) mode to detect HD 189733b. This mode provides imaging photometry at a wavelength (16 μm peak, ~ 5 μm FWHM) intermediate between the 8 μm IRAC and 24 μm MIPS bands. Our PUI photometry began on 17 November 2005 at 23:54 UTC. We placed the star alternately at two positions on the detector array, separated by $25''$(13.5 pixels). We obtained 15 six-second exposures of the star at each position, then nodded to the other position, and repeated this cycle 98 times. We thus acquired a total of 1470 images during the 6-hour observation. The nod procedure allowed us to examine the zodiacal background at each position, out of phase with the stellar observations. This permits us to check the flat-fielding, using the spatially uniform background. The nod also permits measurement of latent image effects, and it provides insurance against unanticipated hot or inoperative pixels.

3. Analysis

3.1. Photometry

The 16 μm zodiacal background in our observations of HD 189733 is approximately 9 MJy/sr, and this is sufficiently weak compared to HD 189733 (peak intensity ~ 250 MJy/sr) to allow simple aperture photometry, not limited by background noise. After eliminating 5 images having obvious flaws, we summed the intensity for each image in a 9×9-pixel box centered on the star, and subtracted the background level. The background level for each image was determined from a histogram of the pixel values outside of the stellar box, fitting a Gaussian to determine the centroid of the histogram. Photometry from the two nod positions differed by a constant factor close to unity (1.005), but showed no other differences above the noise. We normalized the measurements at both nod positions so as to yield the same average intensity.

We also performed aperture photometry on 2MASS20004297+2242342, which is $11''$ distant, and about 4 magnitudes fainter than HD 189733. We set the boundary of the 3×3-pixel box for this comparison star at the intensity minimum between the overlapping PSF

wings of both stars. The comparison star contributes a very small flux in the photometry aperture for HD 189733 ($\sim 0.5\%$), and we corrected for this using a modeled Spitzer PSF.

Figure 1 shows the stellar photometry vs. time for HD 189733, before background subtraction. We record about 10^6 electrons in each exposure, of which $\sim 6.3 \times 10^5$ are from the star. We therefore expect the stellar SNR to be $\frac{6.3\times10^5}{10^3} = 630$. The point-to-point scatter in our final photometry is $\sim 0.0025, SNR \sim 400$. We were not able to improve this significantly by decorrelating against other parameters. For example, we found no significant correlation between the photometric noise and fluctuations in the position of the star on the detector (typically ~ 0.05 pixels, ~ 0.1 arc-sec).

The SNR of our photometry is $\sim$ 60% of the photon noise limit, which is more than sufficient to detect the secondary eclipse of the planet. The eclipse is already obvious as the dip in the time series on Figure 1. A vertical line on the figure at phase 0.5 marks the nominal center of the eclipse. The reality of the eclipse is established by the fact that it is not present in either the comparison star or the background time series. Moreover, the amplitude, central phase, and shape of the eclipse are in close accord with expectations.

3.2. Baseline Fitting

Figure 1 shows that the measured intensity of the star increases steadily over the 6-hour observation sequence. Both the comparison star and the background level show a similar increase, which we denote as the 'ramp'. There are two peak-up arrays in IRS, and the red (22 μm) array (that was pointed to adjacent sky) shows a similar ramp. This ramp is a previously unreported instrument effect, not yet understood by the IRS instrument team. In July 2005 we observed two secondary eclipses of HD 209458 using IRS in the $7 - 14$ μm spectroscopic mode. During these spectroscopic observations, the peak-up arrays (always operating) were both observing adjacent sky, and the backgound in all cases exhibits a similar ramp. We verified that the ramp appears in raw data, so it cannot be an artifact of the pipeline processing at the SSC. We detect very weak latent images after changing the position of HD 189733, but their maximum amplitude (~ 0.002 of the real image) is not sufficient to account for the ramp. It should eventually be possible to diagnose the nature of this ramp, and perhaps correct it from first principles. However, the secondary eclipse is of immediate interest, so here we fit a polynominal to the baseline.

The limiting factor in the accuracy of our secondary eclipse measurement is our ability to correct the ramp, and establish an accurate photometric baseline spanning the eclipse. The ramp has a shape reminiscent of $y \propto ln(\delta t)$, where δt is the elapsed time from start of

observations, but a first-order log function does not fit it particularly well. Moreover, the shape of the ramp is slightly different for sources of different brightness (background, star).

To correct the baseline, we first divide background-subtracted HD 189733 photometry by the comparison star. We do not subtract background from the comparison star, so that it will be a closer match to the intensity level of HD 189733 and also will have greater SNR. It is still necessary to smooth the comparison star photometry, which we do by fitting a fourth-order polynominal in $\ln(\delta t)$ (Figure 1). Dividing HD 189733 by this fit removes virtually all of the higher-order curvature from the HD 189733 time series, for phases greater than 0.45 (neglecting the strongly varying initial measurements). A residual ramp remains in HD 189733 after the division, but it is nearly linear. We zero-weight the eclipse itself ($0.482 \leq \phi \leq 0.518$), and we fit both a linear and a quadratic baseline to the residual ramp in the HD 189733 data.

Our baseline correction has the distinct advantage of not fitting a higher-order polynominal directly to HD 189733 data. Because the eclipse itself must be zero-weighted, the higher-order coefficients would have to be fit 'over the gap', a less robust procedure that we avoid. For investigators who wish to do their own baseline corrections, we include an electronic table (Table 1) giving our photometry both before and after baseline correction. The original data are freely available from the Spitzer Science Center.

4. Results and Discussion

4.1. Stellar Flux

Our background-subtracted photometry yields a stellar flux of 127±8 mJy for HD 189733 at 16 μm. We included an aperture correction of 14%, calculated using a 24 μm MIPS PSF[1] scaled to 16 μm. Our flux error is from calibration scatter described in the IRS Data Handbook[2]. Interpolating in a grid of Kurucz model atmospheres, the flux expected from a 5050/4.5/0.0 model (Bouchy et al. 2005) at 19.3 pc is 104 mJy. The 2MASS K magnitude (=5.54) used with the STAR-PET calculator on the SSC website, for spectral type K2, predicts a stellar flux of 120 mJy. Given the difference between the 16 μm fluxes expected from the 2MASS magnitude, and from a Kurucz model for the Bouchy et al. (2005) temperature, there is no convincing evidence for a circumstellar dust contribution to the 16 μm flux. We therefore interpret the contrast in the secondary eclipse solely in terms

[1]see `http://ssc.spitzer.caltech.edu/mips/psf.html`

[2]`http://ssc.spitzer.caltech.edu/irs/dh/`

of the planet-to-star flux ratio.

4.2. Amplitude of the Secondary Eclipse

Figure 2 shows the baseline-corrected secondary eclipse. We generate a theoretical eclipse curve numerically (Richardson et al. 2006), from the Bouchy et al. (2005) parameters for the system. We fit this to the individual measurements (upper panel of Figure 2). The fit has only two free parameters: phase at center of eclipse, and the eclipse depth. We estimate errors by generating and fitting to 10^4 fake data sets having $\sigma = 0.0025$, matching the scatter in the real data. The standard deviations of the eclipse depth and central phase from these Monte-Carlo realizations are adopted as the errors for these parameters. The best-fit eclipse depth is $0.551\% \pm 0.017\%$, with central phase 0.5026 ± 0.0003. Adopting a stellar flux of ~ 120 mJy, the flux from the planet is ~ 660 μJy.

The exact eclipse depth is dependent on the details of the baseline correction. If we adopt a linear fit over the gap (see above), the derived eclipse depth is 0.521%. The choice between the linear and quadratic baselines is largely subjective; we prefer the quadratic baseline. The magnitude of the difference in eclipse depth for the two choices is indicative of the accuracy of our result, estimated as $\pm 0.03\%$. This being greater than the precision of the detection, baseline correction is the limiting factor in our analysis.

The lower panel of Figure 2 averages the photometry into bins of 0.001 in phase. The eclipse in the binned data is dramatic, and its duration and shape agree well with the theoretical curve. We are aware that some ground-based transit photometry for this planet yields a smaller radius (D. Charbonneau and G. Bakos, private communication). However, the duration of secondary eclipse should be the same as the transit duration, already relatively well determined by the discovery observations. We do not expect that a smaller radius for the planet will affect the duration and shape of the secondary eclipse curve by more than our errors. The brightness temperature inferred for the planet may be more sensitive to radius (see below).

The central phase of the eclipse, 0.5026 ± 0.0003, is seemingly different from 0.5, and at face value this would indicate a non-circular orbit. However, the difference between the discovery orbital period, 2.219 days (Bouchy et al. 2005), and the Hipparcos value we used (2.218575 days, Hebrard & Lecavelier des Estangs 2006; Bouchy et al. 2005), when propagated to the time of our observations, give a phase difference (0.0046) that is greater than the offset we observe. Therefore we regard any conclusions about the central phase of the eclipse as premature until the ephemeris is more firmly established. For reference, our

secondary eclipse is centered at $HJD = 2453692.62416 \pm 0.00067$. Unlike the eclipse depth, the center time does not depend significantly on our baseline correction.

It is interesting to compare this planet with the Spitzer detection of TrES-1 (Charbonneau et al. 2005), since both planets orbit K dwarfs. In thermal equilibrium, and assuming equal Bond albedos and heat re-distribution efficiencies for both planets, their temperatures will scale as:

$$T_p \sim T_s \Delta^{\frac{1}{2}}, \tag{1}$$

where T_s is the effective temperature of the star, and Δ is its angular diameter as seen from the planet. For the TrES-1 (Alonso et al. 2004; Sozetti et al. 2004) and HD 189733 parameters (Bouchy et al. 2005), Eq. (1) predicts virtually identical temperatures, as the larger and hotter star has the more distant planet (TrES-1). The 16 μm brightness temperature of HD 189733, from a Kurucz model, is 4315K. Adopting the Bouchy et al. (2005) ratio of radii, our secondary eclipse contrast translates to a 16 μm brightness temperature for the planet of 1117 ± 42K. This is very similar to both the TrES-1 (1060 ± 50K, Charbonneau et al. 2005) and HD 209458b (1130 ± 150K, Deming et al. 2005) detections. Our contrast measurement is in close accord with a prediction for HD 189733b by Fortney et al. (2006), who expect HD 189733b to be intermediate between TrES-1 and HD 209458b. However, if the planet-to-star radius *ratio* for HD 189733 is revised, then our revised brightness temperature will be:

$$T_p^{16} = 900/\ln(1 + 41.86r^2), \tag{2}$$

where r is the ratio of planet radius to the stellar radius. Our 16 μm measurement is as close to a continuum flux as possible using Spitzer photometry; comparison with the IRAC and MIPS (24 μm) bands (DDT program 261 by D. Charbonneau) should define the degree of absorption by methane, water and CO (Seager et al. 2005; Fortney et al. 2006).

4.3. Beyond the Eclipse Amplitude

The fact that Spitzer detects this secondary eclipse to high SNR (32σ precision) prompts us to ask what other information can be extracted from the eclipse curve, and what are the implications for the detection of lower-mass planets, e.g., hot Neptunes (Bonfils et al. 2005) that may transit.

The lower panel of Figure 2 suggests that our binned data during ingress and egress contain information on the shape of the eclipse curve. The pressure scale height in the atmosphere of a solar-type star (Vernazza et al. 1976) is much less than the radius of a planet. Hence, the shape of the secondary eclipse curve encodes information on the spatial distribution of IR intensity across the planet's disk (Charbonneau et al. 2005). We computed the derivative of intensity with respect to time (phase) for our binned data. We approximate the derivatives as simple finite differences. We fold the eclipse curve about mid-eclipse, averaging ingress and egress, before computing derivatives. Folding maximizes our sensitivity, but smears any planetary thermal structure that is not symmetric.

Figure 3 shows the results for two bin sizes: 0.001 in phase (upper panel), and 0.002 (lower panel). At 0.001 resolution (= 3 minutes) the scatter is much greater than the amplitude of the derivative curve, but the average derivative during ingress/egress is higher than at other phases. As we increase the bin size, the derivatives during ingress/egress must inevitably become significantly different from zero. This follows because the integral of the derivative is the eclipse curve itself, that is already detected to high significance. At 0.002 resolution (6 minutes), the scatter is dramatically improved, the derivatives peak near mid-ingress/egress, and a χ^2 analysis firmly rejects the null hypothesis that the derivatives are consistent with zero (10^{-5} probability). A similar analysis for the comparison star finds only random noise. Apart from the real derivative increase during ingress/egress, only the lower left bin on Figure 3 stands out in the χ^2 analysis, with a 5% probability of being due to noise. This marginal value is due to the extra noise noticeable just before egress, rather than to a real derivative signal. The extra noise can also be seen in the background flucuations at this time (see Figure 1).

Figure 3 compares the observed derivatives to models that are constrained to fit the observed eclipse depth. We use two simple, ad-hoc models: a uniform brightness temperature on the disk (solid line), and an extreme limb-darkened model with intensity falling proportional to $\cos(\theta)$, becoming zero at the limb (dashed line). The dominant effect in the modeled and observed derivatives is the shape of the planet. At 6-minute resolution, the individual derivatives peak at the middle of ingress/egress. The data crudely indicate the overall shape of the planet, but cannot discriminate between a uniform disk (solid line) and the extreme limb-darkened model (dashed line). However, modest improvements in Spitzer duty cycle and SNR may allow us to relax our symmetry assumption, and place meaningful limits on dynamically-forced temperature asymmetries of large spatial scale on the planet's disk (Cho et al. 2003; Cooper & Showman 2005).

The 32σ precision we obtain for this secondary eclipse remains a $> 3\sigma$ detection for a planet an order of magnitude smaller in area, but in an identical orbit. This limit corresponds

to $\sim$ 1 Neptune radius. As we proceed down the main sequence, planet-to-star contrast increases as the inverse square of the stellar radius. For planets orbiting M dwarfs (Bonfils et al. 2005; Rivera et al. 2005; Butler et al. 2004), it follows from Eq. (1) that, in the Rayleigh-Jeans limit, this dominates the reduced heating of the planets. If close-in Neptunes are discovered transiting nearby M dwarfs, their IR emission should be detectable by Spitzer.

This work is based on observations made with the Spitzer Space Telescope, which is operated by the Jet Propulsion Laboratory, California Institute of Technology under a contract with NASA. Support for this work was provided by NASA. We thank Gordon Squires for his rapid handling of our proposal, and the entire Spitzer staff for their efficient scheduling, and rapid data processing. We are grateful to Dave Charbonneau and Gaspar Bakos for discussions concerning this planet, and we thank Daniel Devost, Kevin Uchida, James Houck, and Gregory Sloan for their thoughts regarding IRS systematics. We thank an anonymous referee for comments that improved this paper.

REFERENCES

Alonso, R., and 11 co-authors 2004, ApJ, 613, L15

Barman, T. S., Hauschildt, P. H., & Allard, F. 2005, ApJ, 632, 1132

Bonfils, X., Forveille, T., Delfosse, X., Udry, S., Mayor, M., Perrier, C., Bouchy, F., Pepe, F., Queloz, D., & Bertaux, J.-L. 2005, A&A, 443, L15

Bouchy, F., & 11 co-authors, 2005, A&A, 444, L15

Brown, T. M., Charbonneau, D., Noyes, R. W., & Burrows, A. 2001, ApJ, 552, 669

Burrows, A., Hubeny, I., & Sudarsky, D. 2005, ApJ, 625, L135

Butler, R. P., Vogt, S. S., Marcy, G. W., Fischer, D. A., Wright, J. T., Henry, G. W., Laughlin, G. & Lissauer, J. J. 2004, ApJ, 617, 580

Charbonneau, D., & 10 co-authors, 2005, ApJ, 626, 523

Cho, J. Y.-K., Menou, K., Hansen, B. M. S., & Seager, S. 2003, ApJ, 587, L117.

Cooper, C. S., & Showman, A. P. 2005, ApJ, 629, L45

Deming, D., Seager, S., Richardson, L. J., & Harrington, J. 2005, Nature, 552, 699

Fortney, J. J., Marley, M. S., Lodders, K., Saumon, D., & Freedman, R. 2005, ApJ, 627, L69

Fortney, J. J., Saumon, D., Marley, M. S.,Lodders, K., & Freedman, R. S. 2006, ApJ, in press, astro-ph/0507422

Gaudi, B. S., Seager, S., & Mallen-Ornelas, G. 2005, ApJ, 623, 472

Hebrard, G, & Lecavelier des Estang, A. 2006, A&A, 445, 341

Houck, J. R., & 34 co-authors, 2004, ApJS, 154, 18

Perryman, M. A. C. (ed), 1997, *The Hipparcos and Tycho Catalogues*, ESA SP-1200, European Space Agency, Noordwijk.

Richardson, J. L., Seager, S., Deming, D., Harrington, J., Barry, R. K., Rajagopal, J., & Danchi, W. C. 2006, in IAUC 200, *Direct Detection of Exoplanets: Science & Techniques*, eds. C. Aime, & F. Vakili, in press

Rivera, E. J., Lissauer, J. J., Butler, R. P., Marcy, G. W., Vogt, S. S., Fischer, D. A., Brown, T. M., Laughlin, G., & Henry, G. W. 2005, ApJ, 634, 625

Seager, S., Richardson, L. J., Hansen, B. M. S., Menou, K., Cho, J. Y.-K., & Deming, D. 2005, ApJ, 632, 1122

Sozetti, A., Yong, D., Torres, G., Charbonneau, D., Latham, D. W., Prieto, C. A., Brown, T. M., Carney, B. W., & Laird, J. B. 2004, ApJ, 616, L197

Vernazza, J. E., Avrett, E. H., & Loeser, R. 1976, ApJS, 30, 1

Werner, M. W., & 25 co-authors, 2004, ApJS, 154, 1

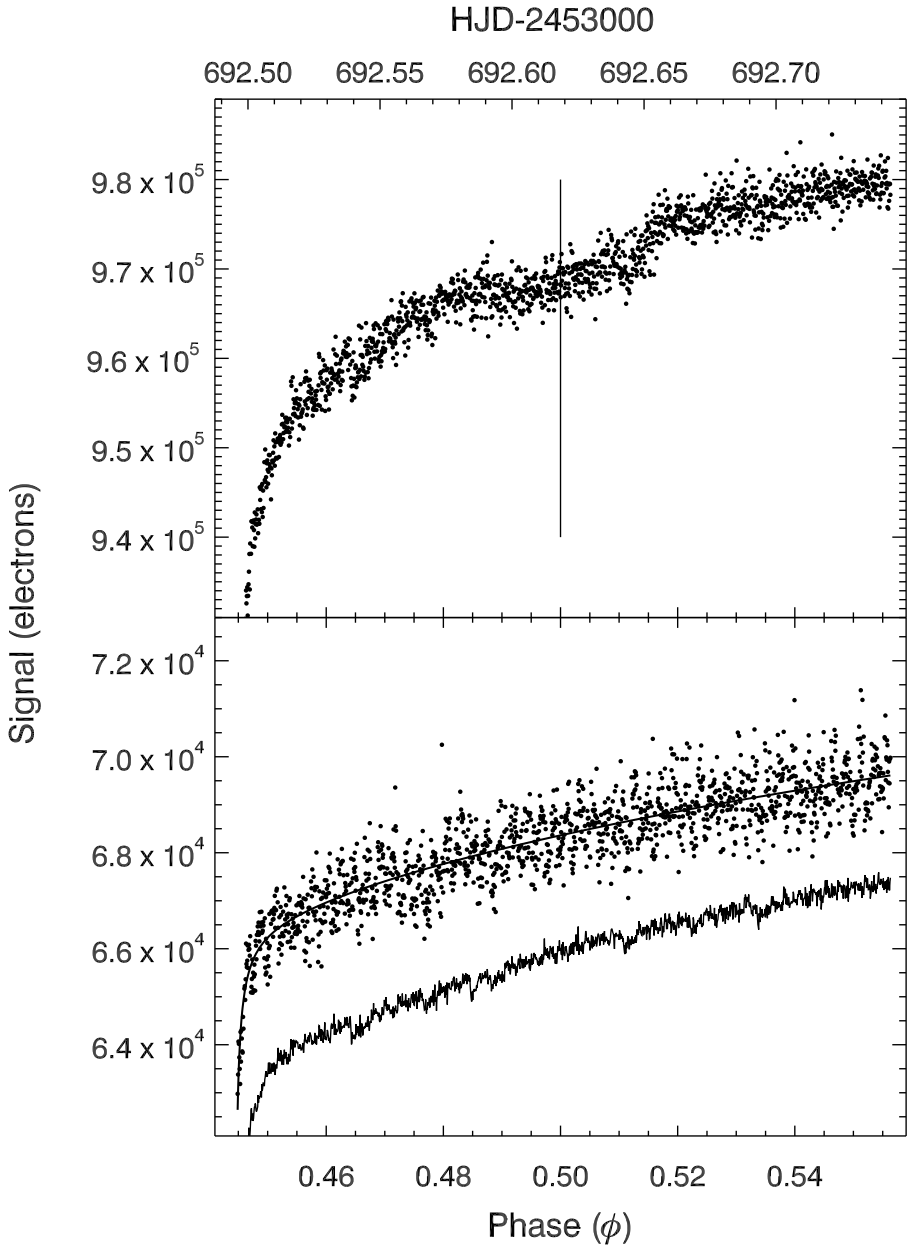

Fig. 1.— *Upper Panel:* Raw aperture photometry, before background subtraction and baseline correction, for HD 189733 versus planetary phase. Note that the secondary eclipse is already visible near phase 0.5 - marked by the vertical line. *Lower Panel:* Aperture photometry of the comparison star (2MASS20004297+2242342, points), with a polynominal fit (solid line through points, see text). The line below the comparison star shows the background level, which has been increased by an arbitrary factor to place it on the same scale. The background in the HD 189733 aperture is about 30% of the total signal, and for the comparison star about 60%.

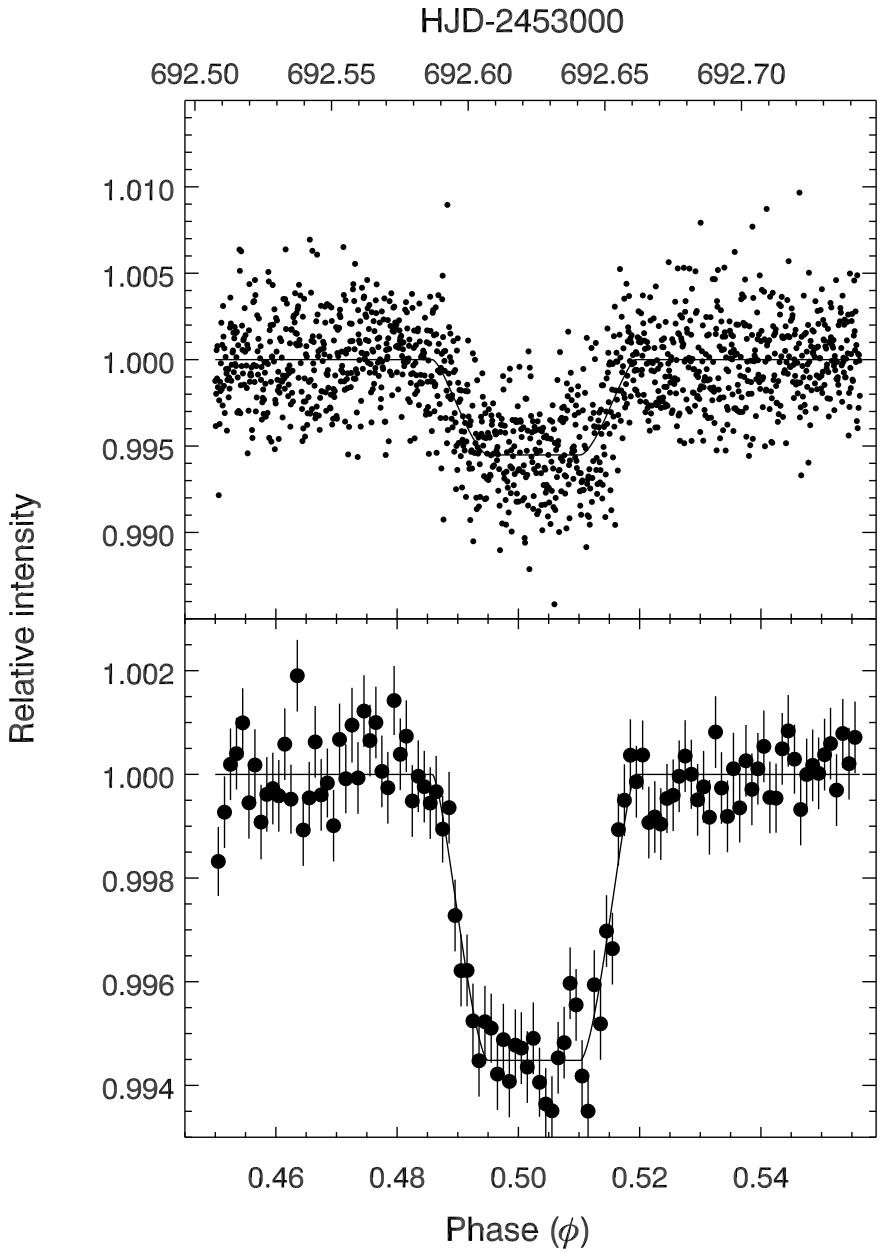

Fig. 2.— *Upper Panel:* Baseline-removed aperture photometry of the HD 189733 secondary eclipse. Points are individual 6-second measurements, with error bars supressed for clarity, but showing the eclipse curve having the best-fit amplitude ($0.551 \pm 0.03\%$) and central phase. *Lower Panel:* Data from the upper panel averaged in bins of width 0.001 in phase ($\sim$ 3 minutes), with error bars and the best-fit eclipse curve.

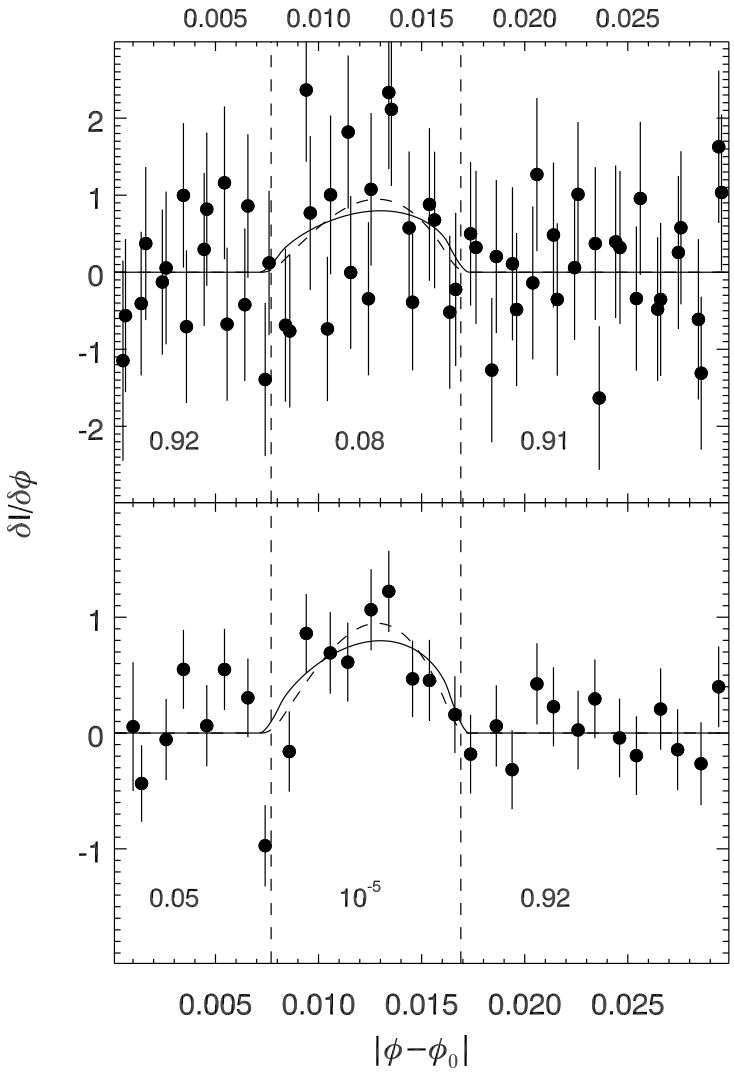

Fig. 3.— *Upper Panel:* Derivative of relative intensity during eclipse with respect to phase (ϕ), versus the absolute phase difference from the center of eclipse (ϕ_0). The derivative values from the data were obtained using a phase resolution of 0.001. The dashed vertical lines indicate the start and end of ingress and egress. *Lower Panel:* Derivative of relative intensity versus phase, as in upper panel, but for a phase resolution of 0.002. The curved line shows the relation expected for a circular planet of uniform brightness temperature, and the dashed line has a temperature distribution sharply peaked at the planet's disk center. The numbers in each region of the figure are the probabilities, from a χ^2 analysis, that the observed derivatives are consistent with zero.

Table 1. Photometry before and after baseline correction. The complete version of this Table is in the electronic edition of the Journal. The printed edition contains only a sample.

	HJD-2453000	Phase	Signal (electrons)	Relative intensity [a]
1	692.49608	0.44488	609247	0.0
2	692.49624	0.44495	610846	0.0
3	692.49639	0.44502	611768	0.0

[a]Baseline-corrected, but given only for phase greater than 0.45